with solids content as high as 40–50% (ref. 27).

As a new paradigm for plastics manufacturing, semi-solid processing of baroplastics raises prospects for the low-temperature moulding of plastics incorporating high-T_g, crystallizing or inorganic components, wherein such hard phases move within a fluidized baroplastic medium. We are currently investigating such systems. By removing the resin-heating and mould-cooling requirements, pressure-based processing could decrease both energy consumption and manufacturing time, while eliminating the thermooxidative degradation that limits plastics recyclability. □

Methods

Block copolymer synthesis

Block copolymers of PS-*b*-PBA and PS-*b*-PEHA were synthesized by atom transfer radical polymerization (ATRP)[20,28,29]. The polystyrene block was first polymerized using methyl-2-bromo-propionate as initiator and CuCl/N,N,N′,N′,N″-pentamethyldiethylene triamine as the catalyst complex in toluene solution at 100 °C. Once the styrene polymerization reached completion, the temperature was lowered to 80 °C and acrylate monomer was added to obtain the second block. The resulting polymer solution was then passed through an alumina column to remove the catalyst and the copolymer precipitated in methanol. The recovered block copolymers were purified by repeated dissolution in dichloromethane followed by precipitation in methanol. The materials were then dried under vacuum followed by freeze-drying from benzene overnight. Compositions and molecular weights of the resulting block copolymers were determined using ^{1}H nuclear magnetic resonance (NMR) and gel permeation chromatography (GPC) based on polystyrene standards.

Core–shell nanoparticle synthesis

Core–shell nanoparticles of PEHA/PS and PBA/PS-d_8 were synthesized by a two-stage microemulsion polymerization technique[23,26]. Tetradecyltrimethylammonium bromide and 2,2′-azobis(2-methylpropionamidine) dihydrochloride were used as emulsifier and initiator, respectively. Polymerization was performed under nitrogen at 65 °C. Acrylate monomer was first added slowly to dionized water in the presence of emulsifier with vigorous stirring and reacted for 15 h. Pre-emulsified styrene was then added slowly to this solution and allowed to react for 3 h. The resulting core–shell particles were precipitated in methanol/water (with a trace amount of NaCl) and washed in DI water several times. The product was then vacuum-dried in the presence of phosphorus pentoxide for three days at room temperature. Compositions and molecular masses were determined as above. Average particle sizes were determined by dynamic light scattering using a Brookhaven Instruments Co. Zeta Potential Analyzer fitted with a 676-nm laser source.

SANS

Measurements were performed at The Manuel Lujan Jr. Neutron Scattering Center at Los Alamos National Laboratory on the Low-*Q* diffractometer, LQD, with the following instrument configuration: wavelength = 1.5–15 Å at 20 Hz, scattering angle = 6–60 mrad on a 59-cm diameter detector, resulting in a q range of 0.003–0.5 Å^{-1}. Samples were ~1-cm-diameter disks of variable thickness. Scattered intensities were corrected for background and thickness in the standard manner.

Received 21 March; accepted 21 October 2003; doi:10.1038/nature02140.

1. Herbst, H., *et al.* in *Frontiers in the Science and Technology of Recycling* (ed. Akovali, G.) 73–101 (Kluwer Academic, Dordrecht, The Netherlands, 1997).
2. Pollard, M., Russell, T. P., Ruzette, A. V., Mayes, A. M. & Gallot, Y. The effect of hydrostatic pressure on the lower critical ordering transition in diblock copolymers. *Macromolecules* **31,** 6493–6498 (1998).
3. Ruzette, A.-V. G., Mayes, A. M., Pollard, M., Russell, T. P. & Hammouda, B. Pressure effects on the phase behavior of styrene/n-alkyl methacrylate block copolymers. *Macromolecules* **36,** 3351–3356 (2003).
4. Ruzette, A.-V. G., Banerjee, P., Mayes, A. M. & Russell, T. P. A simple model for baroplastic behavior in block copolymer melts. *J. Chem. Phys.* **114,** 8205–8209 (2001).
5. Ryu, D. Y., Lee, D. J., Kim, J. K., Lavery, K. A. & Russell, T. P. Effect of hydrostatic pressure on closed-loop phase behavior of block copolymers. *Phys. Rev. Lett.* **90,** 235501 (2003).
6. Hasegawa, H. *et al.* Small-angle neutron scattering studies on phase behavior of block copolymers. *J. Phys. Chem. Solids* **60,** 1307–1312 (1999).
7. Frielinghaus, H., Schwahn, D., Mortensen, K., Almdal, K. & Springer, T. Composition fluctuations and coil conformations in a poly(ethylene-propylene)-poly(ethyl ethylene) diblock copolymer as a function of temperature and pressure. *Macromolecules* **29,** 3263–3271 (1996).
8. Schwahn, D., Frielinghaus, H., Mortensen, K. & Almdal, K. Temperature and pressure dependence of the order parameter fluctuations, conformational compressibility, and the phase diagram of the PEP-PDMS diblock copolymer. *Phys. Rev. Lett.* **77,** 3153–3156 (1996).
9. Russell, T. P., Karis, T. E., Gallot, Y. & Mayes, A. M. Lower critical ordering transition in a diblock copolymer melt. *Nature* **368,** 729–731 (1994).
10. Ryu, D. Y., Jeong, U., Kim, J. K. & Russell, T. P. Closed-loop phase behaviour in block copolymers. *Nature Mater.* **1,** 114–117 (2002).
11. Holden, G. *et al.* in *Thermoplastic Elastomers* (ed. Holden, G.) 573–599 (Hanser, Munich/Vienna/New York, 1996).
12. Ehrenstein, G. H. *Polymeric Materials* 63–89, 98–116 (Hanser, Munich, 2001).
13. Ruzette, A.-V. G. & Mayes, A. M. A simple free energy model for weakly interacting polymer blends. *Macromolecules* **34,** 1894–1907 (2001).
14. Gonzalez-Leon, J. A. & Mayes, A. M. Phase behavior prediction of ternary polymer mixtures. *Macromolecules* **36,** 2508–2515 (2003).
15. Ruzette, A.-V. G. *et al.* Phase behavior of diblock copolymers between styrene and n alkyl methacrylates. *Macromolecules* **31,** 8509–8517 (1998).
16. Hajduk, D. A., Urayama, P., Gruner, S. M. & Erramilli, S. High-pressure effects on the disordered phase of block copolymer melts. *Macromolecules* **28,** 7148–7156 (1995).
17. Hajduk, D. A., Gruner, S. M., Erramilli, S., Register, R. A. & Fetters, L. J. High-pressure effects on the order/disorder transition in block copolymer melts. *Macromolecules* **29,** 1473–1481 (1996).
18. Steinhoff, B. *et al.* Pressure dependence of the order-to-disorder transition in polystyrene/polyisoprene and polystyrene/ poly(methylphenylsiloxane) diblock copolymers. *Macromolecules* **31,** 36–40 (1998).
19. Migler, K. B. & Han, C. C. Static and kinetic study of a pressure-induced order-disorder transition: birefringence and neutron scattering. *Macromolecules* **31,** 300–305 (1998).
20. Patten, T. E. & Matyjaszewski, K. Atom transfer radical polymerization and the synthesis of polymeric materials. *Adv. Mater.* **10,** 901–915 (1998).
21. Malmstrom, E. E. & Hawker, C. J. Macromolecular engineering via 'living' free radical polymerizations. *Macromol. Chem. Phys.* **199,** 923–935 (1998).
22. Hillmyer, M. Block copolymer synthesis. *Curr. Opin. Solid State Mater. Sci.* **4,** 559–564 (1999).
23. Ha, J. W., Park, I. J., Lee, S. B. & Kim, D. K. Preparation and characterization of core–shell particles containing perfluoroalkyl acrylate in the shell. *Macromolecules* **35,** 6811–6818 (2002).
24. Keddie, J. L. Film formation of latex. *Mater. Sci. Eng. R* **21,** 101–170 (1997).
25. Dos Santos, F. D. & Leibler, L. Large deformation films from soft-core/hard-shell hydrophobic latexes. *J. Polym. Sci. B* **41,** 224–234 (2003).
26. Lovell, P. A. & Pierre, D. in *Emulsion Polymerization and Emulsion Polymers* (eds Lovell, P. A. & Aasser, M. S.) 657–695 (John Wiley & Sons, New York, 1997).
27. Flemings, M. C. Behavior of metal alloys in the semisolid state. *Metall. Trans. B* **22,** 269–293 (1991).
28. Shipp, D. A., Wang, J.-L. & Matyjaszewski, K. Synthesis of acrylate and methacrylate block copolymers using atom transfer radical polymerization. *Macromolecules* **31,** 8005–8008 (1998).
29. Cassebras, M., Pascual, S., Polton, A., Tardi, M. & Vairon, J. P. Synthesis of di- and triblock copolymers of styrene and butyl acrylate by controlled atom transfer radical polymerization. *Macromol. Rapid Commun.* **20,** 261–264 (1999).

Acknowledgements We acknowledge the support of the Seaver Institute, the Lord Foundation, Lord Corporation, the MRSEC Program of the National Science Foundation and the Office of Naval Research. This work benefited from the use of the Los Alamos Neutron Science Center at the Los Alamos National Laboratory, funded by the US Department of Energy.

Competing interests statement The authors declare that they have no competing financial interests.

Correspondence and requests for materials should be addressed to A.M.M. (amayes@mit.edu).

Synthetic design of crystalline inorganic chalcogenides exhibiting fast-ion conductivity

Nanfeng Zheng[1], Xianhui Bu[2]* & Pingyun Feng[1]

[1]*Department of Chemistry, University of California, Riverside, California 92521, USA*
[2]*Department of Chemistry, University of California, Santa Barbara, California 93106, USA*

* Present address: Department of Chemistry and Biochemistry, California State University, 1250 Bellflower Blvd, Long Beach, California 90840, USA

Natural porous solids such as zeolites are invariably formed with inorganic cations such as Na^+ and K^+ (refs 1, 2). However, current research on new porous materials is mainly focused on the use of organic species as either structure-directing or structure-building units; purely inorganic systems have received relatively little attention in exploratory synthetic work[3–9]. Here we report the synthesis of a series of three-dimensional sulphides and selenides containing highly mobile alkali metal cations as charge-balancing extra-framework cations. Such crystalline inorganic chalcogenides integrate zeolite-like architecture with high anionic framework polarizability and high concentrations of mobile cations. Such structural features are particularly desirable for the development of fast-ion conductors[10]. These materials demonstrate high ionic conductivity (up to 1.8×10^{-2} ohm^{-1} cm^{-1}) at room temperature and moderate to high humidity. This synthetic methodology, together with novel

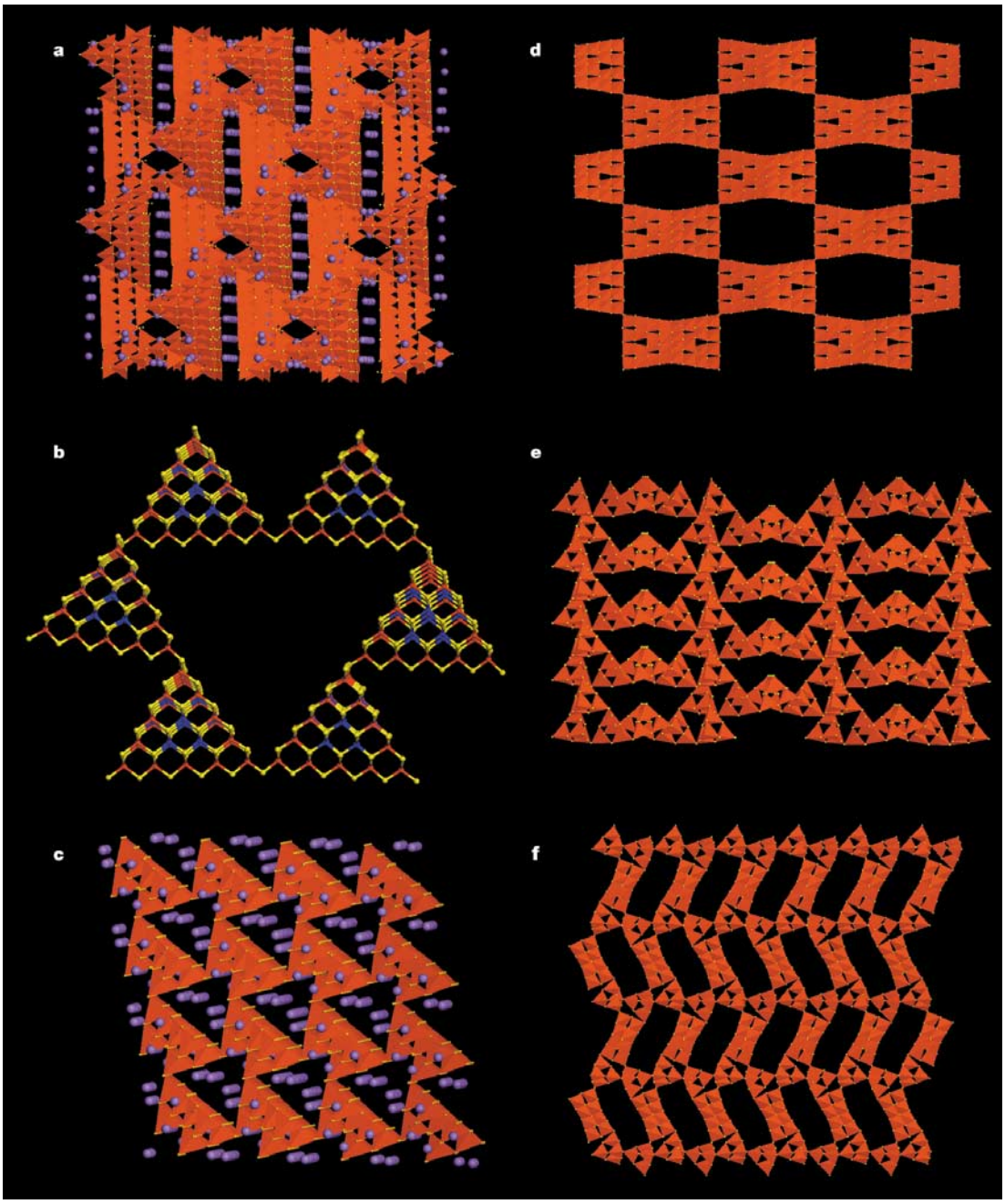

Figure 1 The structural diagrams of the inorganic chalcogenide frameworks. **a**, The 3D diamond-type superlattice in ICF-5 CuInS-Na. Unconnected spheres are Na^+ sites. **b**, The rings formed by six T5 clusters are present in the 3D interpenetrating diamond-type superlattice in ICF-17. **c**, T2 clusters in ICF-21 InSe-Na are connected into a non-interpenetrating diamond-type lattice. Unconnected spheres are Na^+ sites. **d**, The 3D diamond-type superlattice with core-less T4 clusters ($In_{16}S_{32}^{16-}$) in ICF-22 InS-Li. Only one sublattice is shown here for clarity. **e**, The 3D framework of ICF-24 with 20-ring channels. **f**, The 3D framework of ICF-25 with 16-ring channels.

structural, physical and chemical properties, may lead to the development of new microporous and open-framework materials with potential applications in areas such as batteries, fuel cells, electrochemical sensors and photocatalysis.

Commercial applications continue to be dominated by porous materials (for example, zeolites A and X) made from purely inorganic systems. New synthetic methodologies that allow the creation of porous materials from purely inorganic systems will hold great promise for technological applications. One property that could benefit from the compositional and topological features of purely inorganic open-framework chalcogenides is fast-ion conductivity at low temperatures (<100 °C). Fast-ion conductors are useful as electrode materials or solid electrolytes in electrochemical devices such as batteries, fuel cells and sensors. Solids generally have negligible ionic conductivity. Most fast-ion conductors discovered so far have a high conductivity only at high temperatures (>100 °C)[10]. Therefore, the creation of new fast-ion conductors that operate at low temperatures is desirable.

An open-framework material has an inherent advantage for applications such as low-temperature fast-ion conductors because its open channels provide paths for easy ion migration. Unfortunately, zeolites, although they have open channels and cages, are not good fast-ion conductors because of the strong interaction between their oxygen framework and extra-framework charge carriers, such as Li^+ and Na^+ (ref. 2). Open-framework chalcogenides are anticipated to be better ion conductors than zeolites because chalcogen-

Table 1 **A summary of crystallographic data for selected synthesized chalcogenides**

Name	Framework composition	Space group	*a* (Å)	*b* (Å)	*c* (Å)	*R*(*F*)*
ICF-5 CuInS-Na	$Cu_3In_{17}S_{33}^{10-}$	*Fddd*	31.329(9)	32.906(9)	44.546(12)	6.45
ICF-5 CdInS-Na	$Cd_4In_{16}S_{33}^{10-}$	$I4_1/acd$	26.602(4)	26.602(4)	42.660(9)	6.94
ICF-5 MnZnInS-Na	$Mn_{1.8}Zn_{2.2}In_{16}S_{33}^{10-}$	$I4_1/acd$	26.288(8)	26.288(8)	42.637(18)	8.37
ICF-5 CdInS-Li	$Cd_4In_{16}S_{33}^{10-}$	$I4_1/acd$	25.458(2)	25.458(2)	43.471(4)	12.6
ICF-5 ZnInS-Na	$Zn_4In_{16}S_{33}^{10-}$	$I4_1/acd$	26.158(10)	26.158(10)	42.63(2)	13.9
ICF-5 MnInS-Li	$Mn_4In_{16}S_{33}^{10-}$	$I4_1/acd$	24.690(2)	24.690(2)	44.488(5)	7.20
ICF-17 InZnS-Na	$In_{22}Zn_{13}S_{54}^{16-}$	$I4_1/acd$	29.004(9)	29.004(9)	54.53(2)	9.39
ICF-21 InSe-Na	$In_4Se_8^{4-}$	*I*-42*d*	11.765(2)	11.765(2)	22.685(4)	5.55
ICF-22 InS-Li	$In_4S_8^{4-}$	$I4_1/acd$	25.034(7)	25.034(7)	43.506(15)	7.06
ICF-24 InSSe-Na	$In_4S_{2.9}Se_{5.1}^{4-}$	*Fdd*2	28.842(7)	50.035(11)	12.141(3)	6.64
ICF-25 InS-SrCaLi	$In_4S_8^{4-}$	*Fdd*2	28.33(1)	70.31(2)	12.303(4)	6.97
ICF-27 InS-SrLi	$In_{15}S_{29}^{13-}$	$P3_1c$	17.846(3)	17.846(3)	17.333(4)	4.06

*$R(F) = \Sigma||F_o| - |F_c||/\Sigma|F_o|$ with $F_o > 4.0\sigma(F)$.

ides have higher anionic framework polarizability, owing to the large size of S^{2-} or Se^{2-} as compared to O^{2-}. A more polarizable anionic framework will facilitate the migration of mobile cations[10]. Another advantage of open-framework chalcogenides is the high concentration of mobile cations. Chalcogenides can have much more negative frameworks and therefore more charge-balancing cations than zeolites because the framework M^{4+}/M^{3+} (where M is a tetrahedral atom) ratio in chalcogenides can be much smaller than one, whereas it is always larger or equal to one in zeolites or related oxides[11].

Unfortunately, purely inorganic chalcogenides with the zeolite-like architecture do not occur naturally. The limitation of known open-framework chalcogenides is that they are all made by using organic structure-directing agents[12–14]. We have now developed a kinetically controlled synthesis method that has led to the synthesis of hydrated sulphides and selenides with highly mobile alkali or alkaline earth metal cations (for example, Li^+, Na^+, Ca^{2+}) as extra-framework cations (Table 1). Their unprecedented compositions, diverse cluster and crystal structures, and fast-ion conductivity are reported below.

All phases were synthesized from organic-free aqueous solutions under hydrothermal conditions at temperatures below 200 °C (see Methods). As for the synthesis of zeolites, reactions were carried out under highly alkaline conditions. The kinetically controlled processes led to the crystallization of chalcogenides encapsulating mobile inorganic cations in their cavities. These chalcogenides are denoted ICF-*m* (ICF, inorganic chalcogenide framework; *m*, a number related to the type of framework topology). The *m* is often followed by elemental symbols (for example, ICF-21 InSe-Na), indicating in which of several possible framework and extra-framework compositions a particular topology has been made.

Compared to zeolite tetrahedral frameworks, these chalcogenides represent a higher level of the structural hierarchy because they can be derived from simple tetrahedral networks (for example, diamond) by replacing tetrahedral sites with supertetrahedral clusters. Supertetrahedral clusters are regular tetrahedrally shaped fragments of the cubic ZnS-type lattice and are denoted as T*n*, where *n* refers to the number of metal layers[15–17].

A number of 3D framework types have been realized. Here we focus on seven three-dimensional (3D) framework types, denoted ICF-5, ICF-17, ICF-21, ICF-22, ICF-24, ICF-25 and ICF-27. Because of the compositional variations among each topology, over a dozen

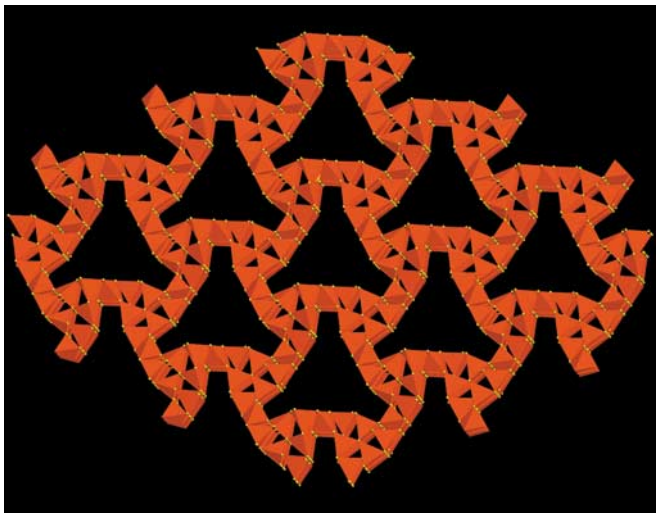

Figure 2 The 3D framework of ICF-27 built from octahedral cluster units.

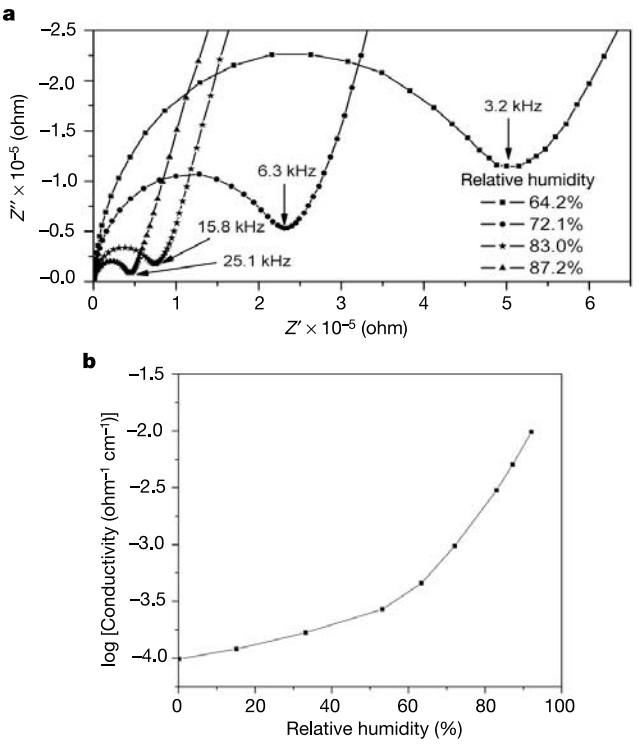

Figure 3 The dependence of the ionic conductivity on the relative humidity for ICF-5 CuInS-Na. **a**, Complex impedance plots under different relative humidities. The data were measured on a single crystal sample at 18 °C. Before each measurement, the sample was kept under the given humidity for 2 h. Z' and Z'' are the real and imaginary parts of the impedance, respectively. **b**, The ionic conductivity of the same sample under different relative humidities.

different materials have been prepared and structurally determined by single-crystal X-ray diffraction (Supplementary Information). That the large supertetrahedral T4 (in ICF-5, Fig. 1a) and T5 (in ICF-17, Fig. 1b) clusters could be prepared from inorganic systems is an important step towards the development of novel clusters. Before this work, chalcogenide clusters were usually synthesized in the presence of organic ligands or bases that serve either to stabilize the cluster surface or to balance the charge on clusters.

In ICF-5, T4 clusters ($M_{20}S_{33}^{10-}$) are joined together into two interpenetrating lattices (Fig. 1a). ICF-5 can be made in diverse chemical compositions with either lithium or sodium as extra-framework cations (Table 1). ICF-17 contains the largest supertetrahedral cluster (for example, $Zn_{13}In_{22}S_{54}^{16-}$) made from M^{2+} and M^{3+} cations (Fig. 1b). In this cluster, M^{2+} cations are distributed at the core and faces of the cluster whereas higher-charged In^{3+} cations terminate the cluster surface at the edges and corners of the cluster. These T5 clusters resemble the core–shell nanoparticles. ICF-21 InSe-Na (formula $NaInSe_2{\cdot}xH_2O$) with the T2 cluster $In_4Se_8^{4-}$ is the first hydrated selenide with the 4-connected, 3D framework (Fig. 1c). Its structure is distinct from the anhydrous $NaInSe_2$ that has a layered structure with octahedral In^{3+} cations[18].

In ICF-22, core-less T4 clusters ($In_{16}S_{32}^{16-}$) are assembled into two interpenetrating lattices (Fig. 1d). The core-less T4 cluster is similar to the ordinary T4 cluster (for example, $Zn_4In_{16}S_{33}^{10-}$) except that the core sulphur atom and its adjacent four metal (for example, Zn_4S^{6+}) atoms are missing.

One prominent structural feature in ICF-24 and ICF-25 is the presence of rings with three T2 clusters. At the other extreme, rings of ten T2 clusters in ICF-24 represent the largest-known ring size formed by supertetrahedral clusters (Fig. 1e). ICF-24 is the first 4-connected, 3D framework structures with a ring size of 20. In comparison, the ring size in ICF-25 is 16, made of eight T2 clusters (Fig. 1f). As in ICF-21, both ICF-24 and ICF-25 have 3D non-centrosymmetric framework structures. ICF-27 can be considered as a 6-connected network with the $In_{18}S_{41}^{28-}$ cluster as the pseudo-octahedral building unit. The $In_{18}S_{41}^{28-}$ clusters are cross-linked in three dimensions by edge-sharing InS_4 tetrahedra at six corners (Fig. 2).

One notable difference from zeolites is the chemical compositions in which the above topological features are realized. ICF-21 InSe-Na, ICF-22 InS-Li, ICF-24, and ICF-25 are the first examples of zeolite-like, 4-connected, 3D open-framework chalcogenides built without tetravalent cations. They represent extreme cases that demonstrate the fundamental difference between oxides and chalcogenides. Zeolite-like oxides generally follow the Loewenstein rule that states that the ratio of M^{4+}/M^{3+} must be larger than or equal to one.

The non-compliance with the Loewenstein rule can lead to a higher concentration of mobile charge carriers in chalcogenides than in zeolites. For a zeolite, not only are M^{4+} cations required in the framework, but the ratio of M^{4+} to M^{3+} cations has to be larger than or equal to one (for example, $NaAlSiO_4{\cdot}xH_2O$). This limits the maximum number of monovalent charge-balancing cations to 0.5 per framework tetrahedral cation. On the other hand, the M^{4+}/M^{3+} ratio in 4-connected, 3D chalcogenides can be less than one (ref. 11). Even the extreme limit ($M^{4+}/M^{3+} = 0$) can be realized, as shown here. The lower M^{4+}/M^{3+} ratio leads to a more negative framework and a higher concentration of extra-framework mobile cations. There can be up to one monovalent charge carrier per tetrahedral cation in chalcogenides (compared to the maximum value of 0.5 in zeolites and related oxides). A high concentration of charge carriers will help enhance ionic conductivity.

The integration of the open-framework architecture with high framework polarizability and high concentration of charge carriers gives rise to a high ionic conductivity in these chalcogenides. The specific conductivity of ICF-5 CuInS-Na is $1.2 \times 10^{-2}\,\mathrm{ohm^{-1}\,cm^{-1}}$ at 18 °C under 100% relative humidity (Fig. 3a, b) (see Methods). A high value is also observed in the selenide ICF-21 InSe-Na with the specific conductivity of $3.4 \times 10^{-2}\,\mathrm{ohm^{-1}\,cm^{-1}}$ at 21 °C under 100% relative humidity (Fig. 4a, b). Of particular interest is the high ionic conductivity observed in one lithium-containing

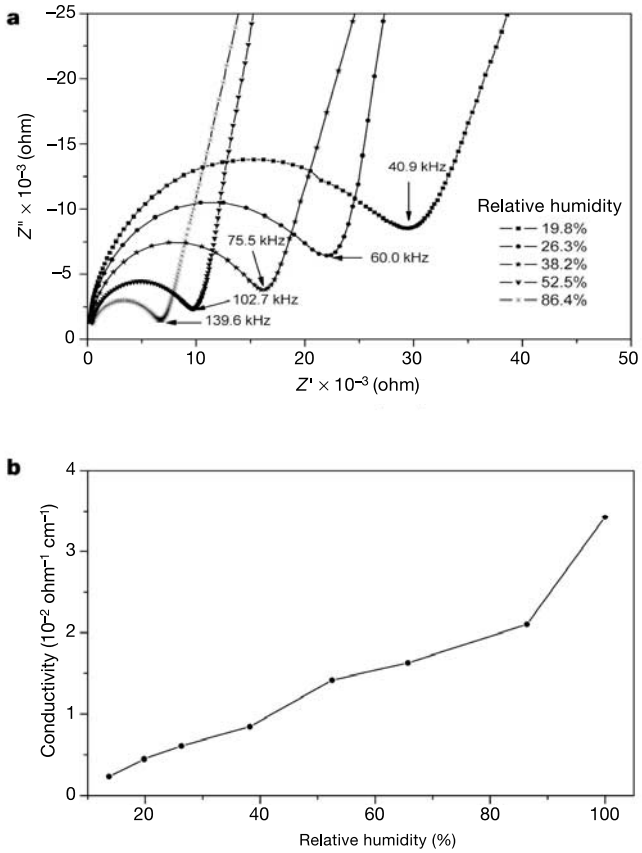

Figure 4 The dependence of the ionic conductivity on the relative humidity for ICF-21 InSe-Na. **a**, Complex impedance plots at 21 °C under different relative humidities. **b**, The ionic conductivity under different relative humidities.

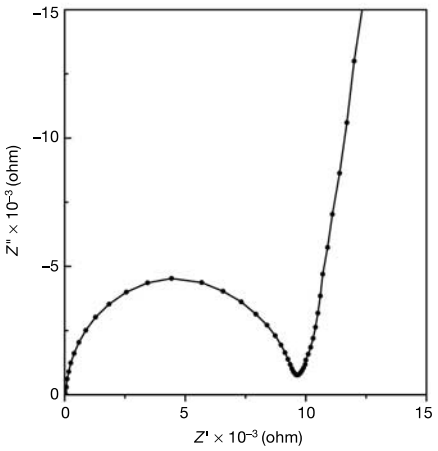

Figure 5 The a.c. impedance plot of ICF-22 InS-Li at 24.0 °C under 31.7% relative humidity. The area of the cross-section for the pellet is $3.83 \times 10^{-3}\,\mathrm{cm^2}$ and the length is 0.405 cm. The sample resistance from this plot is 9572.2 Ω. The specific conductivity is $1.1 \times 10^{-2}\,\mathrm{ohm^{-1}\,cm^{-1}}$.

material, ICF-22 InS-Li (Supplementary Information). Its specific conductivity reaches up to 1.1×10^{-2} ohm^{-1} cm^{-1} at 24 °C under 31.7% relative humidity (Fig. 5). The ionic conductivity of these chalcogenides generally increases with the relative humidity. For example, at 18 °C, the conductivity of ICF-5 CuInS-Na ranges from 1.0×10^{-4} ohm^{-1} cm^{-1} under 0.2% relative humidity to 1.2×10^{-2} ohm^{-1} cm^{-1} under 100% relative humidity (Fig. 3a, b). A similar trend is observed for ICF-21 InSe-Na (Fig. 4a, b).

Despite their high ionic conductivity, there are some limitations for the practical applications of these materials, particularly for lithium batteries, because a relative humidity of 30% or higher is needed to achieve the highest ionic conductivity. Another possible application might take advantage of the open architecture and narrow bandgaps (as compared to oxides) of these materials for photocatalysis. In either case, further research is needed to develop these materials for practical applications.

The materials reported are probably only a small group of a much larger family of inorganic open-framework chalcogenides. The synthetic method described here should be applicable to a range of chalcogenide structures and compositions. The diverse chemical compositions and crystal structures provide rich opportunities in exploring the physical and chemical properties of these chalcogenides and in establishing structure–property relationships. □

Methods

Typical synthesis conditions are given below using ICF-22 InS-Li, ICF-21 InSe-Na, and ICF-5 CuInS-Na as examples.

For ICF-22 InS-Li, $In(NO_3)_3{\cdot}H_2O$ (339.2 mg), LiCl (176.9 mg), Li_2S (210.3 mg), and H_2O (2.1967 g) were mixed and stirred in a 23-ml Teflon-lined stainless steel autoclave for 20 min. The vessel was then sealed and heated at 190 °C for 4 days. After cooling to room temperature, a ~68% yield of colourless crystals was obtained.

For ICF-21 InSe-Na, a mixture of $In(NO_3)_3{\cdot}H_2O$ (381.5 mg), Na_2Se (408.3 mg), and H_2O (2.0240 g) was prepared and stirred in a 23-ml Teflon-lined stainless steel autoclave for 10 min. The vessel was then sealed and heated at 170 °C for 3 days. The autoclave was cooled to room temperature. A ~77% yield of pale-yellow octahedral crystals was obtained.

For ICF-5 CuInS-Na, $In(NO_3)_3{\cdot}H_2O$ (372.0 mg), $Cu(NO_3)_2{\cdot}3H_2O$ (67.98 mg), Na_2S (234.4 mg), and water (2.5740 g) were mixed in a 23-ml Teflon-lined stainless steel autoclave and stirred for 10 min. The vessel was then sealed and heated at 150 °C for 3 days. After cooling to room temperature, a ~85% yield of red crystals was obtained.

For ICF-5 CuInS-Na, the elemental analysis (wt%) was 44.22 In, 4.03 Cu (calculated 43.97 In, 4.29 Cu) based on the formula $Na_{10}[Cu_3In_{17}S_{33}]{\cdot}56(H_2O)$. The thermal analysis shows that ICF-5 CuInS-Na undergoes a total of 17.0% water loss in the temperature range from room temperature to 200 °C. All crystal structures were solved from single crystal data collected at 150 K on a SMART 1000 charge-coupled device (CCD) diffractometer.

Ionic conductivities were measured by a.c. impedance methods with an applied frequency range of 10 to 20 MHz using a Solartron 1260 frequency response analyser. Both pellet and single crystal samples were used for measurements. Pellets were prepared by compressing the fresh powder sample at the pressure of 5,000 psi and were then cut into smaller pellets shaped like the rectangular prism. Liquid gallium was used as contacting electrodes.

Received 4 May; accepted 27 October 2003; doi:10.1038/nature02159.

1. Flanigen, E. M. in *Introduction to Zeolite Science and Practice* (eds van Bekkum, H., Flanigen, E. M. & Jansen, J. C.) 13–34 (Elsevier, New York, 1991).
2. Breck, D. W. *Zeolite Molecular Sieves, Structure, Chemistry, and Use* (John Wiley & Sons, New York, 1974).
3. Davis, M. E. Ordered porous materials for emerging applications. *Nature* **417,** 813 (2002).
4. Feng, P., Bu, X. & Stucky, G. D. Hydrothermal syntheses and structural characterization of zeolite analogue compounds based on cobalt phosphate. *Nature* **388,** 735–741 (1997).
5. Scott, R. W. J., MacLachlan, M. J. & Ozin, G. A. Synthesis of metal sulfide materials with controlled architecture. *Curr. Opin. Solid State Mater. Sci.* **4,** 113–121 (1999).
6. Huo, Q., Leon, R., Petroff, P. M. & Stucky, G. D. Mesostructure design with gemini surfactants: supercage formation in a three-dimensional hexagonal array. *Science* **68,** 1324–1327 (1995).
7. Zhao, D. *et al.* Triblock copolymer syntheses of mesoporous silica with periodic 50 to 300 angstrom pores. *Science* **279,** 548–552 (1998).
8. Johnson, S. A., Ollivier, P. J. & Mallouk, T. E. Ordered mesoporous polymers of tunable pore size from colloidal silica templates. *Science* **283,** 963–965 (1999).
9. Cheetham, A. K., Ferey, G. & Loiseau, T. Open-framework inorganic materials. *Angew. Chem. Int. Edn* **38,** 3268–3292 (1999).
10. West, A. R. *Solid State Chemistry and its Applications* (Wiley, New York, 1992).
11. Zheng, N., Bu, X. & Feng, P. Microporous and photoluminescent chalcogenide zeolite analogs. *Science* **298,** 2366–2369 (2002).
12. Bedard, R. L., Wilson, S. T., Vail, L. D., Bennett, J. M. & Flanigen, E. M. in *Zeolites: Facts, Figures, Future. Proc. 8th Int. Zeolite Conf.* (eds Jacobs, P. A. & van Santen, R. A.) 375 (Elsevier, Amsterdam, 1989).
13. Cahill, C. L. & Parise, J. B. On the formation of framework indium sulfides. *J. Chem. Soc. Dalton Trans.* 1475–1482 (2000).
14. Dhingra, S. & Kanatzidis, M. G. Open framework structures based on Se_x^{2-} fragments: synthesis of $(Ph_4P)[M(Se_6)_2]$ (M = Ga, In, Tl) in molten $(Ph_4P)_2Se_x$. *Science* **258,** 1769–1772 (1992).
15. Li, H., Laine, A., O'Keeffe, M. & Yaghi, O. M. Supertetrahedral sulfide crystals with giant cavities and channels. *Science* **283,** 1145–1147 (1999).
16. Wehmschulte, R. J. & Power, P. P. Low-temperature synthesis of aluminum sulfide as the solvate $Al_2S_6(NMe_3)_4$ in hydrocarbon solution. *J. Am. Chem. Soc.* **119,** 9566–9567 (1997).
17. Bu, X., Zheng, N., Li, Y. & Feng, P. Pushing up the size limit of chalcogenide supertetrahedral clusters: two- and three-dimensional photoluminescent open frameworks from $(Cu_5In_{30}S_{54})^{13-}$ clusters. *J. Am. Chem. Soc.* **124,** 12646–12647 (2002).
18. Hoppe, R., Lidecke, W. & Frotath, F. C. Sodium thioindate and sodium selenoindate. *Z. Anorg. Allgem. Chem.* **309,** 49–54 (1961).

Supplementary Information accompanies the paper on **www.nature.com/nature**.

Acknowledgements We acknowledge the support of this work by the NSF. We also thank Y. Yan and his group for assistance with impedance measurements.

Competing interests statement The authors declare that they have no competing financial interests.

Correspondence and requests for materials should be addressed to P. F. (pingyun.feng@ucr.edu).

Explosive volcanism may not be an inevitable consequence of magma fragmentation

Helge M. Gonnermann & Michael Manga

Earth and Planetary Science, University of California, Berkeley, California 94720, USA

The fragmentation of magma, containing abundant gas bubbles, is thought to be the defining characteristic of explosive eruptions[1–3]. When viscous stresses associated with the growth of bubbles and the flow of the ascending magma exceed the strength of the melt[2,4–6], the magma breaks into disconnected fragments suspended within an expanding gas phase. Although repeated effusive and explosive eruptions for individual volcanoes are common[7,8], the dynamics governing the transition between explosive and effusive eruptions remain unclear. Magmas for both types of eruptions originate from sources with similar volatile content, yet effusive lavas erupt considerably more degassed than their explosive counterparts[7,8]. One mechanism for degassing during magma ascent, consistent with observations, is the generation of intermittent permeable fracture networks generated by non-explosive fragmentation near the conduit walls[9–11]. Here we show that such fragmentation can occur by viscous shear in both effusive and explosive eruptions. Moreover, we suggest that such fragmentation may be important for magma degassing and the inhibition of explosive behaviour. This implies that, contrary to conventional views, explosive volcanism is not an inevitable consequence of magma fragmentation.

Analysis of pumice samples from the explosive eruption of Mount Pinatubo, 15 June 1991, suggests that non-newtonian rheology and growth of gas bubbles during magma ascent led to intense shear and possibly fragmentation at the conduit walls[9]. Recent observations suggest that fragmentation at the conduit walls may not be restricted to explosive eruptions. Tuffen *et al.*[10] describe multiple generations of tuffisite veins in the dissected vent of a rhyolite lava flow at Torfajökull, Iceland. They[10] interpret these features to record repeated cycles of brittle fragmentation followed by annealing of the fragments and subsequent deformation of the reannealed magma by viscous flow, to form flow banding. Textures within the tuffisite veins suggest that fragmentation created a

